GEOFLUIDS

Geofluids (2013) **13**, 101–111 doi: 10.1111/gfl.12009

Synchrotron XRF and XANES investigation of uranium speciation and element distribution in fluid inclusions from unconformity-related uranium deposits

A. RICHARD[1], J. CAUZID[1,2], M. CATHELINEAU[1], M.-C. BOIRON[1], J. MERCADIER[1] AND M. CUNEY[1]

[1]*GéoRessources, Université de Lorraine, CNRS, CREGU, Vandoeuvre-lès-Nancy, France;* [2]*European Synchrotron Radiation Facility, Grenoble, France*

ABSTRACT

Fluid inclusions from two quartz samples of the McArthur River and Rabbit Lake unconformity-related uranium deposits (Athabasca Basin, Canada) were analysed by synchrotron X-ray fluorescence (SXRF) and X-ray absorption near-edge spectroscopy (XANES) to shed light on (i) the detailed chemistry of the fluids having transported the uranium and (ii) the speciation of uranium in these fluids. The analysed samples contain variable proportions of NaCl-rich or $CaCl_2$-rich (25–35 wt% salts) fluid inclusions that homogenise into the liquid phase between 120 and 200°C. For unknown reason, all of the $CaCl_2$-rich fluid inclusions decrepitate under X-ray beam after a few seconds, precluding any SXRF or XANES measurement. SXRF on 12 homogenised NaCl-rich fluid inclusions from the Rabbit Lake sample shows that the fluid inclusions contain appreciable amounts of Br, Fe, Sr, transition metals (Mn, Ni, Cu, Zn), Pb, U and rare earth elements (REE) (La, Ce), with concentrations being relatively homogeneous among fluid inclusions. Within the complex McArthur River sample (numerous fluid inclusions + randomly distributed solids), statistical analyses of hyperspectral SXRF images were performed using the non-negative matrix approximation (NNMA) method. This strategy allows distinguishing the three domains contributing to the overall signal: (i) the quartz matrix, which notably contains significant amounts of Cr, Cu and Pb; (ii) the fluid inclusions characterised by high amounts of Br, Fe, Sr and transition metals; and (iii) La-Ce ± Fe solids. Part of the U and REE are spatially associated with distinct optically invisible solids within the quartz matrix. XANES on four McArthur River sample fluid inclusions at room temperature and at 150°C (fluid inclusion trapping temperature) as well as in solid and liquid U(IV) and U(VI) standards, respectively, shows that the uranium has remained in the form of U(VI) from trapping to present in the fluid inclusion.

Key words: Athabasca Basin, fluid inclusions, speciation, synchrotron, unconformity, uranium

Received 16 July 2012; accepted 9 November 2012

Corresponding author: Antonin Richard, GéoRessources, Université de Lorraine, CNRS, CREGU, Boulevard des Aiguillettes B.P. 70239, F-54506, Vandoeuvre-lès-Nancy, France.
Email: antonin.richard@univ-lorraine.fr. Tel: +33 3 83 68 47 25. Fax: +33 3 83 68 47 01

Geofluids (2013) **13**, 101–111

INTRODUCTION

Uranium is a redox-sensitive element that can be readily transported in the form of soluble uranyl $(U^{6+}O_2)^{2-}$ complexes in a variety of geological fluids and precipitates mainly in the form of U(VI) or U(IV) minerals in a large diversity of geological environments (Cuney 2009; Hazen *et al.* 2009). The case of giant unconformity-related U deposits from the Proterozoic Athabasca Basin (Saskatchewan, Canada) documents (i) a highly efficient process of U concentration over five orders of magnitude between the average continental crust (approximately 1 ppm) and the deposits (up to 20% U on average) and (ii) drastic changes in redox conditions during the U transport (more oxidising) and deposition (more reducing) as pitchblende (UO_2) (see Jefferson *et al.* (2007), Kyser & Cuney (2008) and Boiron *et al.* (2010) for reviews of genetic models).

In previous works, significant effort was made to use fluid inclusions to understand the origin of the mineralising fluids, their chemistry and the conditions for U transport in the Athabasca U deposits. The fluids responsible for mineralisation and alteration of the surrounding crystalline and sedimentary rocks were identified by the widespread occurrence of high-salinity fluid inclusions (25–35

wt% salts) observed in quartz and dolomite veins, quartz cements in the sandstones and healed microfractures (i.e. secondary fluid inclusion planes) in quartz from gneisses and pegmatoids (e.g. Pagel *et al.* 1980; Kotzer & Kyser 1995; Derome *et al.* 2005; Mercadier *et al.* 2010; Richard *et al.* 2010, 2012). The fluid inclusion chemistry was investigated in detail by using laser-induced breakdown spectroscopy (LIBS) and laser ablation - inductively coupled plasma - mass spectrometry (LA-ICP-MS). Na-Ca-Mg-K-Sr-Ba-U compositions of fluid inclusions were obtained, showing well-defined mixing trends between a NaCl-rich brine and a $CaCl_2$-rich brine end-member (Derome *et al.* 2005; Richard *et al.* 2010). The U content of the fluid inclusions is highly heterogeneous at the sample scale (<0.2 to approximately 600 ppm) irrespective of the brine chemistry. This particular feature could be alternatively interpreted as reflecting (i) the actual heterogeneity of the brine U content before UO_2 deposition or (ii) ongoing UO_2 precipitation at the time of fluid inclusion trapping (Richard *et al.* 2012).

In this context, obtaining the spatial distribution of trace elements and U speciation in fluid inclusion and their surrounding matrix could provide crucial information on (i) the origin of the brines; (ii) the fluid–rock interactions they underwent and (iii) the conditions for uranium transport and deposition. Promising synchrotron experiments on Athabasca fluid inclusions were carried out by McCready *et al.* (2005, 2006), although no quantification of inclusion chemistry was performed. The present paper shows (i) elemental distribution in fluid inclusions and their host quartz as well as quantitative fluid inclusion compositions determined by synchrotron X-ray fluorescence (SXRF) (e.g. Philippot *et al.* 2000; Cauzid *et al.* 2006) and (ii) direct measurement of U speciation at room temperature and in homogenised fluid inclusions placed in a heating/freezing stage by X-ray absorption near-edge spectroscopy (XANES) (e.g. Cauzid *et al.* 2007) and tried here at the U-L3 edge. The sampling was focussed on two samples from two classical and extensively studied deposits, McArthur River and Rabbit Lake. Thus, the results and conclusions presented here have general implication for unconformity-related uranium deposits.

GEOLOGY, SAMPLING AND FLUID INCLUSION SELECTION

Regional geology

The Athabasca basement rocks consist of Archaean gneisses, Paleoproterozoic metapelites and mafic to felsic intrusions, which were strongly metamorphosed (up to approximately 800°C and approximately 800 MPa) during the approximately 2.0 to approximately 1.9 Ga Thelon-Talston orogeny in the west, and the approximately 1.9 to approximately 1.8 Ga Trans-Hudson orogeny in the east (Fig. 1) (Chiarenzelli *et al.* 1998; Annesley *et al.* 2005; Card *et al.* 2007).

The unmetamorphosed Athabasca Basin unconformably overlies the crystalline basement and was deposited from 1.76 Ga (Ramaekers *et al.* 2007). The present-day maximum thickness of the sedimentary cover is approximately 1.5 km, but it is thought to have reached a maximum thickness of approximately 5 km, based on P-T estimates from fluid inclusion studies (Derome *et al.* 2005). The basal sediments hosting the U ores consist of an approximately 1-km-thick sequence of fluvial to marginal marine quartz-rich sandstones known as the Fair Point and Manitou Falls Formations (Ramaekers *et al.* 2007).

Unconformity-related U deposits

The unconformity-related U ores are located at the interface between the Athabasca Basin, its underlying crystalline basement and basement-rooted faults crosscutting the unconformity (Fig. 1). The characteristic sequence of alteration associated with U ores (including the studied deposits) is (i) partial to complete replacement of basement biotite, K-feldspar, plagioclase and hornblende by illite + sudoite (Mg-chlorite) ± dravite (Mg-tourmaline), and precipitation of illite and sudoite in sandstone porosity; (ii) dissolution of quartz and finally; and (iii) precipitation of dravite + quartz ± haematite ± pitchblende ± dolomite in veins, vugs and cementing breccias (e.g. Derome *et al.* 2005; Mercadier *et al.* 2010, 2012). U-Pb ages on pitchblende indicate that multiple episodes of mineralisation and/or recrystallisation of the ores occurred

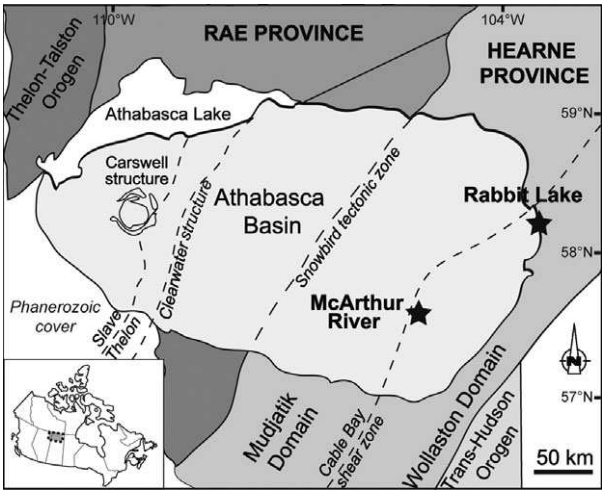

Fig. 1. Simplified geological map of the Athabasca Basin and its underlying basement, with location of the two studied unconformity-related U deposits. Basement domains are individualised by different shades of grey. Modified from Jefferson *et al.* (2007) and Card *et al.* (2007).

between 1.6 Ga and 1.1 Ga (e.g. Cumming & Krstic 1992; Fayek *et al.* 2002; Alexandre *et al.* 2009).

The fluid inclusions studied here were sampled in quartz veins from two well-characterised deposits of the Athabasca Basin: Rabbit Lake and McArthur River (Fig. 1). These deposits share the typical mineralogical, structural and fluid inclusion characteristics of unconformity-related U deposits described above (Hoeve & Sibbald 1978; Pagel *et al.* 1980; Heine 1986; Kotzer & Kyser 1995; Alexandre *et al.* 2005; Derome *et al.* 2005).

Rabbit Lake deposit sample

The Rabbit Lake sample was collected in a barren zone in the hanging wall of the basement-rooted reverse fault that underlies the mineralisation. The sample consists of a barren quartz–dolomite vein (Fig. 2A) crosscutting altered basement gneisses, one of the typical basement lithologies found in the Rabbit Lake area along with dolomitic marbles, plagioclasite and granite pegmatite (Hoeve & Sibbald 1978; Heine 1986; Alexandre *et al.* 2005). At Rabbit Lake, the mineralisation is typically hosted by quartz–dolomite breccias or veins similar to the studied sample, the occurrence of UO_2 being not systematic in these structures (Hoeve & Sibbald 1978; Heine 1986; Alexandre *et al.* 2005).

The Rabbit Lake sample was selected to specifically investigate the fluid inclusion chemistry using SXRF. This sample contains no visible mineral inclusions and shows a number of relatively large fluid inclusions (Fig. 2C) also as described in Pagel *et al.* (1980). The fluid inclusions are of both NaCl-rich and $CaCl_2$-rich brine composition, and U has been detected by LA-ICP-MS in the <0.3 to approximately 230 ppm range (see Richard *et al.* (2012) were this sample is referred as RBL1Qz). Therefore, the studied fluids relate to U-bearing mineralising fluids. The overall good quality of this sample and fluid inclusions has motivated detailed SXRF investigation of fluid inclusions.

McArthur River deposit sample

The McArthur River sample was collected from a position in direct contact with high-grade U ore (>10 wt% U) in the footwall of the basement-rooted reverse fault that structurally controls the mineralisation (Kotzer & Kyser 1995; Alexandre *et al.* 2005; Derome *et al.* 2005). The sample consists of a quartz–dolomite vein filling a sudoite and pitchblende-rich breccia (Fig. 2B) (see detailed description in Derome *et al.* (2005) where this sample is referred as H459-33). This assemblage is hosted by metapelites, one of the typical basement lithologies in this deposit along with metaquartzite (Kotzer & Kyser 1995; Alexandre *et al.* 2005; Derome *et al.* 2005).

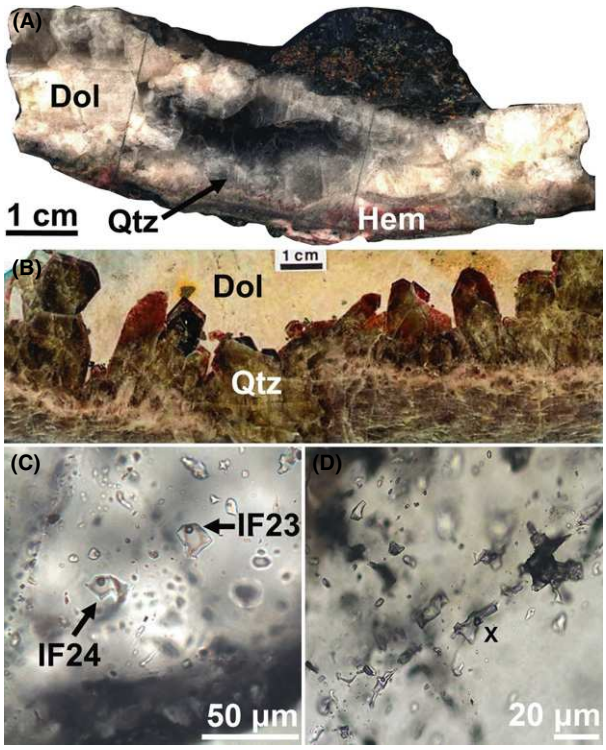

Fig. 2. Samples and fluid inclusions selected for synchrotron investigation in Athabasca unconformity-related U deposits. (A) Rabbit Lake deposit sample showing quartz and dolomite filling fracture in altered gneiss. (B) McArthur River deposit sample showing quartz and dolomite filling a sudoite and pitchblende-rich breccia (not in the picture, see detailed description in Derome *et al.* (2005) where this sample is referred as H459-33). (C) Typical quartz-hosted primary two-phase (liquid + vapour) fluid inclusions in the Rabbit Lake sample selected for synchrotron X-ray fluorescence (SXRF) analysis (see microthermometric and compositional data corresponding to IF23 and IF24 among others in Table 1). (D) Fluid inclusion-rich zone in quartz from the McArthur River sample selected for SXRF mapping (see Fig. 4 for results of SXRF mapping; the 'X' mark shows correspondence with Fig. 4). Qtz, quartz; Dol, dolomite; Hem, haematite.

The McArthur River sample was selected to establish elemental distribution and U speciation in fluid inclusions and their host quartz by SXRF mapping and XANES, respectively. It has been shown that the quartz matrix of this sample contains some U-rich zones that are probably due to tiny U-rich solid inclusions (Richard *et al.* 2010). This sample contains fluid inclusions (Fig. 2D) in which the U concentration determined by LA-ICP-MS is <0.2 to approximately 600 ppm (Richard *et al.* 2010). Hence, the potential for different U species and occurrences at the sample scale has motivated SXRF mapping of this complex (numerous fluid inclusions + randomly distributed solids) sample and XANES measurements on U-rich fluid inclusions detected by SXRF mapping. Due to beamtime limitations, the time allocated to SXRF mapping was the minimum necessary to detect the presence of U and other elements. For this reason, no quantitative data are

presented for the McArthur River sample inclusions (only for the Rabbit Lake sample).

Fluid inclusion selection

Prior to synchrotron experiments, Rabbit Lake and McArthur River quartz samples hosting fluid inclusions were prepared as sections of approximately 200 μm thickness polished on top and bottom faces. The inclusions targeted are located between 10 and 100 μm below the quartz surface and have a density of approximately 1.25 due to their high salinity. The samples are dominated by 5–25 μm, two-phase (liquid + vapour) and three-phase (liquid + vapour + halite) primary and pseudosecondary fluid inclusions (Fig. 2C,D). The volume fraction of the vapour phase is typically close to 10%.

For the McArthur River sample, comprehensive fluid inclusion data have been reported by Derome *et al.* (2005). This sample contains fluid inclusions of both NaCl- and $CaCl_2$-rich brine compositions. The fluid inclusions were not systematically re-investigated by microthermometry here.

For the Rabbit Lake sample, microthermometry was carried out on fluid inclusions using a Linkam MDS600 heating/freezing stage. The temperatures of phase changes were measured for the following: eutectic melting (T_e), ice melting (T_m ice), hydrohalite melting (T_m hyd), halite dissolution (T_s NaCl) and homogenisation by vapour disappearance (T_h). According to the calibration curves, temperatures of phase changes were measured with an accuracy of about ±5°C for Te and ±0.1°C for T_m ice, T_m hyd, T_s NaCl and T_h. The fluid inclusions in the Rabbit Lake sample show microthermometric characteristics comparable to those from McArthur River sample (Derome *et al.* 2005). Therefore, the fluid inclusions have been classified and their salinity calculated following the nomenclature and phase relations in the H_2O-NaCl-$CaCl_2$ system used by Derome *et al.* (2005) for the McArthur River deposit. Briefly, the fluid inclusions have a restricted range of salinity of approximately 25–35 wt% salts, and large variation of cation composition (molar Na/Ca between 2 and 20). All fluid inclusions homogenise into the liquid phase generally between 120 and 200°C. Of the 22 inclusions selected for SXRF analysis, 12 have microthermometric behaviour typical of the NaCl-rich brine inclusions and the other 10 inclusions behave like the $CaCl_2$-rich ones. Microthermometric data are reported in Table 1 for NaCl-rich brine fluid inclusions only (see Section SXRF experiments for explanation).

SYNCHROTRON XRF AND XANES METHODS

Synchrotron X-ray fluorescence analyses were performed on beamline ID22 of the European Synchrotron Radiation Facility (ESRF) in its first hutch (Martinez-Criado *et al.* 2012) as part of the experiment EC561. The beamline was equipped with a flat Si mirror and a Si(111) crystal monochromator ($\Delta E/E = 10^{-4}$). The monochromatic 17.2 keV X-ray beam was focussed by KB mirrors onto the sample in a 2 × 5 μm² (vertical × horizontal) spot. The photon flux onto the sample was approximately 10^{11} ph s^{-1}, monitored by a mini-ionisation chamber. The samples were positioned in the focal plane with a visible light microscope and held vertically in the beam by a heating/freezing HFS91 Linkam stage providing an analytical temperature range of −196°C to 600°C (simplified from Cauzid *et al.* 2007).

Fluorescence detection was made with a Vortex Si-drift detector set at 90° from the incident beam in the polarisation plane. Step size was similar to that of the spot (2 × 5 μm² [vertical × horizontal]) so that areas of interest were entirely analysed. The experimental setup was calibrated using NIST standards (SRM1832, SRM1833), and synthetic liquids sealed in fused silica glass capillaries (1000 ppm $CuCl_2$, $FeCl_2$, $ZnCl_2$ or $PbCl_2$). Fluorescence fitting and elemental images were performed using the PyMca software (Solé *et al.* 2007). Statistical analyses of hyperspectral images were performed using the non-negative matrix approximation (NNMA, Lee & Seung (1999)) module available in PyMca.

Due to tiny crystals interfering with transmission measurements (Cauzid *et al.* 2004), inclusion thickness determination was hampered. This parameter mainly consists in a dilution factor on each quantified element. Therefore, the results were limited to elemental ratios to remove the effect of inclusion thickness on the quantification procedure. Inclusion depth in the host was determined optically. Indirect depth estimation using Kα/Kβ ratios relies on low-energy elemental fluorescence lines (Philippot *et al.* 1998), which usually are restricted to S, Cl, K and Ca. In our case, those elements either had concentrations that were too low to be used or absorption by the host quartz that was too high for deep inclusions. Inclusion depth within the host crystal and inclusion thickness are the two main error sources in the quantification procedure. Based on error propagation calculations (Cauzid *et al.* 2006), it has been shown that inclusion depth mainly affects elements quantified using a fluorescence line of low energy (≤6 keV) and becomes negligible for elements quantified using a fluorescence line of high energy (≥8 keV). The reverse behaviour is observed with the inclusion thickness: negligible for elements quantified using a fluorescence line of low energy (≤6 keV) and becomes dominant for elements quantified using a fluorescence line of high energy. The same study (Cauzid *et al.* 2006) also showed that using the internal standard quantification procedure does not provide the lowest error bars but is less sensitive to how these two parameters are evaluated. The expected errors (1σ) on a single fluid inclusion decrease from 70%

Table 1 Microthermometric data and element concentrations determined by synchrotron X-ray fluorescence (SXRF) for the NaCl-rich brine fluid inclusions in the Rabbit Lake sample. See Section Synchrotron XRF and XANES methods for estimation of analytical errors on element concentrations. Values preceded by a < symbol stand for the limit of detection when the element was not detected. Temperatures of phase changes during microthermometric experiments: eutectic melting (T_e), ice melting (T_m ice), hydrohalite melting (T_m hyd) and homogenisation by vapour disappearance (T_h). Element concentrations in NaCl-rich brine fluid inclusions determined by laser ablation - inductively coupled plasma - mass spectrometry (LA-ICP-MS) (10 inclusions) are shown for comparison (after Richard *et al.* 2010). nd, not determined.

IF no.	T_e (°C)	T_m ice (°C)	T_m hyd (°C)	T_h (°C)	NaCl (wt%)	$CaCl_2$ (wt%)	Salinity (wt%)	K (ppm)	Ca (ppm)	Cr (ppm)	Mn (ppm)	Fe (ppm)	Ni (ppm)	Cu (ppm)	Zn (ppm)	Sr (ppm)	Cs (ppm)	Ba (ppm)	La (ppm)	Ce (ppm)	Pb (ppm)	U (ppm)
IF7	−67	−26.0	−8.3	175.9	15.3	12.5	27.8	200	20 000	200	200	500	20	20	100	900	50	20	20	70	80	<3
IF9	−60	−25.6	−0.9	130.3	17.0	11.9	28.9	2000	20 000	800	200	1400	70	50	90	700	60	200	200	500	100	10
IF13	−62	−25.3	−7.4	155.8	17.0	11.3	28.2	600	20 000	300	400	1000	30	20	100	800	100	200	80	20	60	4
IF18	−59	−25.5	−10	139.5	16.2	11.6	27.8	1000	20 000	400	200	1300	30	30	100	800	20	100	200	200	60	<5
IF19	−58	−24.6	−2.4	149.9	19.3	9.9	29.1	70	20 000	600	200	1000	40	50	70	500	90	100	100	90	50	<5
IF22	−62	−24.1	0.7	121.6	20.9	8.7	29.7	600	50 000	900	60	1200	40	30	100	600	1100	500	9000	20 000	90	<6
IF23	−67	−26.0	4.8	221.7	16.8	12.6	29.5	5000	30 000	600	200	1000	50	30	100	600	70	100	90	300	80	<6
IF24	−72	−25.9	0.4	132.8	16.5	12.4	29.0	900	10 000	1000	20	1700	60	30	70	800	1200	700	9000	20 000	100	7
IF33	−66	−24.6	−16.9	130.9	17.5	9.8	27.3	3000	10 000	1000	300	2000	90	50	100	800	40	200	200	300	100	7
IF34	−67	−24.5	−12.5	185.3	18.3	9.6	27.9	600	10 000	400	300	800	30	20	100	800	4	9	300	700	100	<4
IF35	−67	−24.1	−10.5	141.8	19.6	8.7	28.3	2000	70 000	500	300	1300	40	30	100	800	40	60	50	300	80	<5
IF38	−60	−25.1	−1.9	150.1	18.1	10.9	29.0	1000	20 000	600	200	2000	50	40	100	500	80	100	100	200	200	4
						SXRF	μ (ppm)	1400	20 000	600	200	1300	50	30	90	700	50*	100*	100*	300*	90	6
						This study	± 1 σ (%)	90	70	40	50	30	40	30	10	20	50*	60*	60*	70*	40	40
						LA-ICP-MS	μ (ppm)	2000	30 000	nd	250	520	nd	70	100	500	4	200	nd	nd	20	2
						Richard *et al.* (2010)	± 1 σ (%)	40	20	nd	50	30	nd	120	nd	30	100	80	nd	nd	50	70

*The μ ± 1σ (%) concentrations of Ba, Cs, Ce and La in NaCl-rich brine fluid inclusions determined by SXRF do not take into account the data from IF22 and IF24.

to 40% on elements quantified using a fluorescence line of low energy (in the following order: Cl, K, Ca, Cs, Ba, La, Ce, Mn, Fe) and reach a constant value of 30% on elements quantified using a fluorescence line of higher energy (Ni, Cu, Zn, Sr, Pb, U). Quantification was performed using the method of Cauzid *et al.* (2006) and counter-checked with PyMca. Both methods provided similar results within error bars.

X-ray absorption near-edge spectroscopy measurements were performed in fluorescence mode with the same setup at the U-L3 edge (17.166 keV). The monochromator energy was calibrated using Pb (L1 edge, 15.861 keV) and Zr (K edge, 17.998 keV) extended X-ray absorption fine structure (EXAFS) foils. Energy scans were performed from 17.1 to 17.74 keV, with a 0.5 eV resolution from 17.14 to 17.34 keV and lower energy resolution below 17.14 keV (1 eV) and above 17.34 keV (2 eV) for normalisation purposes. Fluorescence signal was measured during one second at each energy point. XANES standards consisted in (i) massive and unaltered (approximately 1 mm^2) solid pitchblende (UO_2) from the Millennium uranium deposit (Athabasca Basin), similar to that described in Cloutier *et al.* (2009), prepared as thin section and (ii) liquid standard of 8.5 molal LiCl, $UO_2(NO_3)_2$ (10^{-2} mol l^{-1}), pH = 1–2 adjusted with HNO_3, sealed in fused silica glass capillary. These two XANES standards were used for U(IV) and U (VI) valence states, respectively.

RESULTS

Decrepitation of $CaCl_2$-rich fluid inclusions

Without exception, all of the $CaCl_2$-rich brine fluid inclusions from both samples decrepitate under X-ray beam after a few seconds. This phenomenon occurs at room temperature as well as at 250°C. This precludes any SXRF or XANES measurement on $CaCl_2$-rich brine fluid inclusions. To our knowledge, such behaviour during synchrotron experiments has not been reported before, even in previous experiments on similar samples and fluid inclusions carried out at beam line L at the Hamburger Synchrotronstrahlungslabor (HASYLAB, Hamburg, Germany) (McCready *et al.* 2005, 2006). At this stage, the cause for decrepitation is unknown. Therefore, all the results reported below concern NaCl-rich fluid inclusions only.

SXRF experiments

For the Rabbit Lake sample, a series of 12 NaCl-rich brine fluid inclusions were analysed by SXRF once homogenised at 250°C. Homogenisation ensures that all elements occur as dissolved species in the liquid phase. During homogenisation, complete redissolution of any precipitated phases was checked using fluorescence mapping. For each inclusion, XRF spectra were collected for 2000 sec real time. All calculated elements were statistically above background signal, while the overlapping peaks were deconvoluted using PyMca (Solé *et al.* 2007). The elements detected were K, Ca, Cr, Mn, Fe, Ni, Cu, Zn, Br, Sr, Cs, Ba, La, Ce, Pb and U (note that elements lighter than K are hardly detected using SXRF). The elements concentrations were normalised to that of Br, which is the most incompatible quantified element (i.e. could hardly be present as mineral inclusions in the quartz matrix and is only present in the fluid inclusions). This element was therefore used as an internal standard in the quantification procedure (Ménez *et al.* 2002; Cauzid *et al.* 2006). Br concentration was previously estimated by bulk crush leach coupled with ion chromatography and LA-ICP-MS analysis (Richard *et al.* 2011; Leisen *et al.* 2012). The Athabasca inclusions show a relatively constant Br content of 2000 ± 500 ppm, and this value was used to calculate the absolute element concentrations in the fluid inclusions reported in Table 1 and Fig. 3. U was only detected in five inclusions (4–10 ppm); others displayed calculated concentrations slightly below their limit of detection (3–6 ppm). The fluid inclusions contain appreciable amounts of Cr (200–1000 ppm), Ni (20–90 ppm), Ce (20–700 ppm) and La (20–300 ppm). Two inclusions (IF22 and IF24) show anomalously high calculated Ce and La content (20 000 and 9000 ppm, respectively).

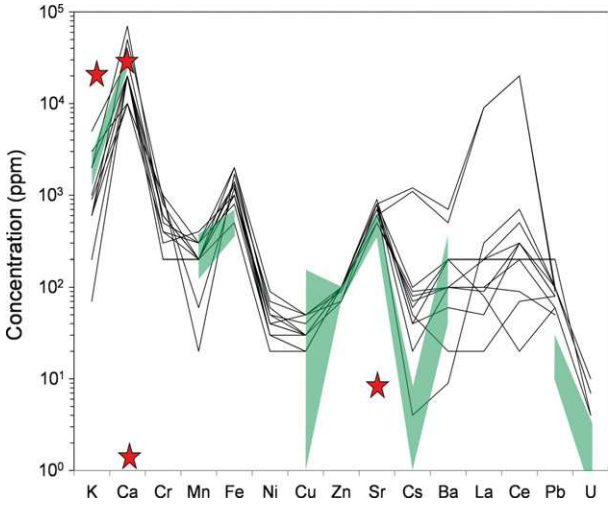

Fig. 3. Composition of the NaCl-rich brine fluid inclusions from the Rabbit Lake sample determined by synchrotron X-ray fluorescence (SXRF). The μ ± 1σ element concentrations of NaCl-rich brine fluid inclusions determined by laser ablation - inductively coupled plasma - mass spectrometry (LA-ICP-MS) (10 inclusions) are shown in green for comparison (after Richard *et al.* 2010). Raw data are shown in Table 1. Red stars indicate the possible composition of epsomite-saturated evaporated seawater from which the Athabasca brines originate (see Section Insights from fluid inclusion composition for details). Compositions of evaporated seawater are from Fontes & Matray (1993) and Lowenstein & Timofeeff (2008). The lower and upper values for Ca concentration in evaporated seawater are for $MgSO_4$ seas and $CaCl_2$ seas, respectively.

For the McArthur River sample, the result of SXRF elemental mapping at room temperature and NNMA data processing on a selected fluid inclusion-rich zone are shown in Fig. 4, and the fluorescence spectra of the domains (vectors) contributing to the overall signal are shown in Fig. 5. Three domains can be identified: (Vector 0) the quartz matrix (in blue), which notably contains significant amounts of Cr, Cu and Pb; (Vector 1) the fluid inclusions (in green) characterised by high amounts of Br, Fe, Sr and transition metals and (Vector 2) La-Ce ± Fe solids (in red) randomly distributed within the matrix and possibly associated to some fluid inclusions. The low average signal of U and Rb do not appear in those vectors. The La-Ce ± Fe solids could not be identified optically because of parallax and in-depth analysis, coupled with high abundance of fluid inclusions and microfractures, which precludes locating easily the objects identified by SXRF mapping. U was found to be concentrated as hot spots probably in some tiny solids and not dissolved in the liquid part of fluid inclusions. However, it was not possible to perform XANES on these U-rich tiny solids because their occurrence has been revealed after the experiments during data processing.

XANES experiments

In the McArthur River sample, four U-bearing fluid inclusions (checked by fluorescence mapping) were selected in a zone different from that shown in Figs 2D and 4. After SXRF, no quantification was possible (dissolved U below approximately 5 ppm). Figure 6 shows the results of the XANES experiments on the fluid inclusions and on liquid U(VI) and solid U(IV) standards. The XANES signals of the four selected inclusions are highly reproducible and therefore only one signal representative of the four signals

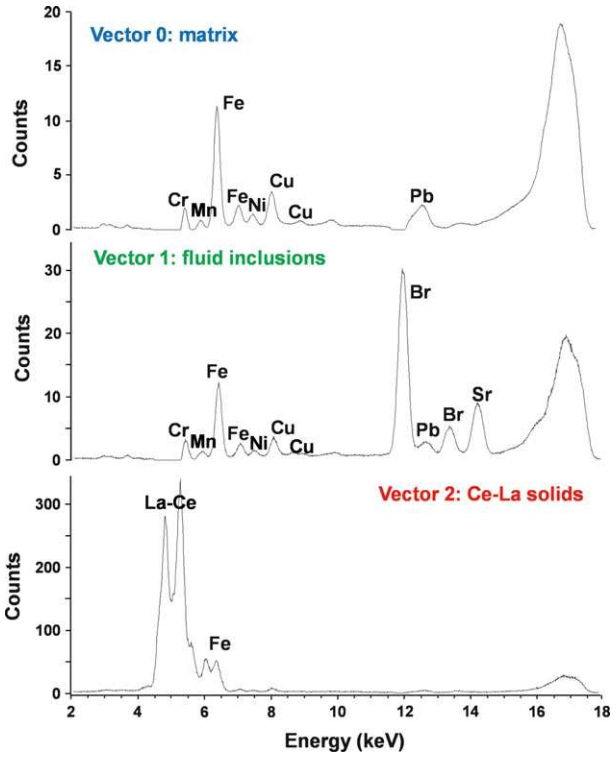

Fig. 5. Synchrotron X-ray fluorescence (SXRF) spectra associated with the three main vectors from non-negative matrix approximation (NNMA) in the McArthur River sample. See Fig. 4 for correspondence with NNMA chemical mapping of fluid inclusions in the same zone: Vector 0: matrix (in blue); Vector 1: fluid inclusions (in green) and Vector 2: Ce-La solids (in red).

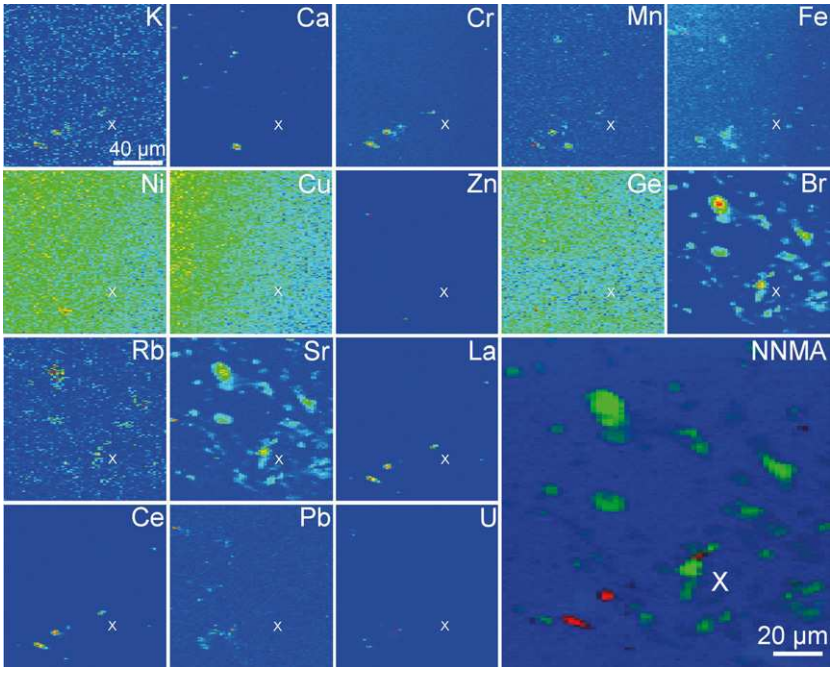

Fig. 4. Synchrotron X-ray fluorescence (SXRF) maps of one fluid inclusion-rich zone in the McArthur River sample. Same scale applies to all SXRF maps. The 'X' mark shows correspondence between maps and Fig. 2D. Note that parallax and in-depth sample analysis tends to deform objects and apparent distances between them. NNMA: result of non-negative matrix approximation (NNMA) chemical mapping of fluid inclusions in the same zone. Blue: matrix; green: fluid inclusions; red: Ce-La solids. Colours were adjusted to minimum and maximum values for each individual map. Fluorescence spectra associated with the three main vectors from NNMA are shown in Fig. 5.

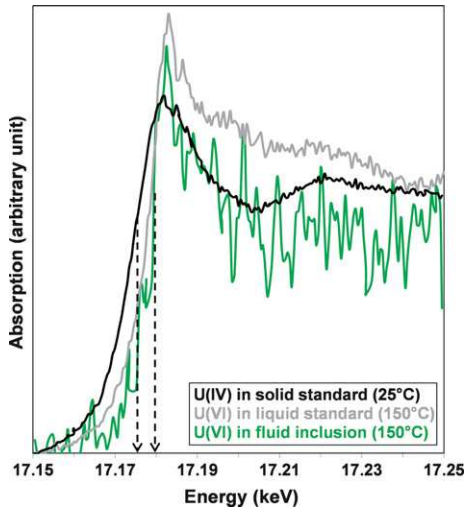

Fig. 6. X-ray absorption near-edge spectroscopy (XANES) spectra acquired on homogenised U-bearing fluid inclusions from the McArthur River sample and U(IV) and U(VI) standards. 150°C approximates the trapping temperature of fluid inclusions. Before normalisation, raw signals were, in the 17.2–17.25 keV energy range, of 4000 counts in the U(VI) standard (solution in capillary), 20 000 counts in the U(IV) standard (solid UO_2) and approximately 900 counts in natural samples. The signals of the four selected inclusions are highly reproducible between 25°C and 150°C and therefore only one representative signal acquired is presented. Dotted arrows indicate the U-edge positions: approximately 17.174 keV for solid U(IV) standard and approximately 17.179 keV for fluid inclusions and liquid U(VI) standard.

acquired is presented in Fig. 6. This fluorescence signal is measured on the U-L3 edge (17.166 keV), which provides a fluorescence line at 16.428 keV. At this energy, even at 100 μm depth, absorption in quartz will be less than 10%. The signal is of poor quality mainly because U concentration is very low in most fluid inclusions. The edge positions were calculated using the maximum of the first differential. Despite noisy signals, it appears that U edges of fluid inclusions show no variation (approximately 17.179 keV) between 25°C and 150°C (approximate fluid inclusion trapping temperature at McArthur River after Derome *et al.* 2005). At 150°C, complete homogenisation of fluid inclusions was checked using fluorescence mapping. As expected, liquid U(VI) and solid U(IV) standards have clearly distinct edge positions (approximately 17.179 keV and approximately 17.174 keV, respectively). Comparison with U edges of standards is subject to caution but may indicate that the U in fluid inclusions remains in the form of U(VI) at every tested conditions.

DISCUSSION

Insights from fluid inclusion compositions

For the Rabbit Lake sample, the calculated concentrations for K, Ca, Cr, Mn, Fe, Ni, Cu, Zn, Sr, Cs, Ba, La, Ce, Pb and U in NaCl-rich brine fluid inclusions show significant variation (one to two orders of magnitude). This can be partly attributed to analytical uncertainty. However, none of the fluid inclusion displays clearly atypical composition (except for the anomalously high Cs, Ba, Ce and La content in IF22 and IF24, which could be partly attributed to tiny solids positioned above or below the inclusions). Therefore, the population analysed appears to be relatively homogeneous and may provide a viable estimation of the composition of the NaCl-rich brine in the Rabbit Lake deposit (Table 1; Fig. 3). The composition of the NaCl-rich brine fluid inclusions found here may relate to the Br-Sr-Fe ± U-Pb-Ce or to Br-Sr ± Cu-Ni-Pb-Zn-Fe fluid inclusions identified using SXRF by McCready *et al.* (2005, 2006). However, direct comparison is not possible because the elements concentrations are not provided in the latter studies.

The composition of the NaCl-rich brine fluid inclusions obtained by SXRF in the Rabbit Lake sample compares rather well with that obtained by LA-ICP-MS on the McArthur River NaCl-rich brine fluid inclusions (Table 1; Fig. 3). Therefore, it can be reasonably assumed that both techniques lead to comparable results and that the NaCl-rich brine is relatively homogeneous in composition in the two studied deposits, the minor differences of Cs and U concentration being possibly attributable to local particularities. Although SXRF does not allow detection of elements lighter that K, an advantage of the technique compared to LA-ICP-MS is that there is no need to select the elements of interest before analysis. Here, SXRF on the studied samples shows that the NaCl-rich brine fluid inclusions contain dissolved solutes like Cr, Ni, Ce and La, which were not tested in previous LA-ICP-MS works (Richard *et al.* 2010, 2012).

As shown by Cl/Br and δ^{37}Cl analysis of fluid inclusions and δ^{11}B analysis of dravite, the NaCl- and $CaCl_2$-rich brines originate from evaporation of seawater up to epsomite saturation (Richard *et al.* 2011; Leisen *et al.* 2012; Mercadier *et al.* 2012). Here, the possible composition of epsomite-saturated evaporated seawater from which the Athabasca brines originate is plotted in Fig. 3 (Fontes & Matray 1993; Lowenstein & Timofeeff 2008). The K and Sr compositions of the NaCl-rich brine fluid inclusions are clearly shifted from their original ones. The case of Ca is more contentious and depends on the chemistry of the initial seawater, which may have been either $MgSO_4$ rich (as present-day seawater) or $CaCl_2$ rich (Lowenstein & Timofeeff 2008). As a whole, the data suggest that fluid–rock interaction has been an important control on the composition of the NaCl-rich brine and is a possible explanation to its high metal content.

In the McArthur River sample, the occurrence of uranium as tiny mineral inclusions in the quartz matrix confirms what was suspected from previous LA-ICP-MS analyses (Richard *et al.* 2010). Ce and La are widely

known for being highly mobile in the environment of the studied deposits (e.g. Fayek & Kyser 1997; Gaboreau *et al.* 2007; Mercadier *et al.* 2011). The REE are thought to be leached by the brines from monazite, which shows spectacular alteration features in basement rocks (Hecht & Cuney 2000). The REE are redistributed among aluminium phosphate-sulphate (APS) minerals and pitchblende in the altered and mineralised zones. Here, the presence of La-Ce ± Fe solids within the quartz matrix and of La and Ce in the fluid inclusions is consistent with REE mobility associated with brine circulation. Although the nature of the La-Ce ± Fe solids within the quartz matrix could not be properly identified, a reasonable hypothesis is that these solids represent mixtures of APS and haematite co-precipitated with quartz. The high concentration of Ce (20–700 ppm) and La (20–300 ppm) within the fluid inclusions and the association of fluid inclusion hosting quartz with REE-bearing solids suggest that the high REE concentration in the fluid inclusions provides a first-order approximation of the REE-mineral solubility in the brines.

In both Rabbit Lake and McArthur River samples, the presence of Ni within fluid inclusions is consistent with the occurrence of Ni sulphides and arsenides typically found in relatively small amounts in the ore mineralogy and associated with other sulphide and arsenide minerals containing Fe, Ni, Co, Cu, Pb, Zn, As, Mo and occasionally Au, Ag, Se and platinum group elements (Ruzicka 1989). The precise paragenetic position of these minerals with respect to U deposition has remained unclear. However, they are clearly spatially associated with U ores (Ruzicka 1989), and the presence of Ni in the fluid inclusions supports the idea that the precipitation of sulphide and arsenide minerals is related to the same brines as the precipitation of U ores. Ni is typical of mafic lithologies, which are not recognised close (approximately 1 km) to the studied deposits, but well documented, however, in the Athabasca Basement (Annesley *et al.* 2005). If Ni and U are really brought to the mineralised bodies by the same brines, this would imply a relatively large-scale circulation of the brines within basement rocks. The occurrence of Cr is more enigmatic with regard to the scarcity of Cr in the country rocks and the absence of Cr in the ore mineralogy.

Implication for uranium transport and speciation

The widespread presence of haematite and the absence of magnetite in the vicinity of the investigated uranium deposits suggest that the oxygen fugacity (f_{O2}) in the system should have been well above the haematite/magnetite buffer ($\log f_{O2} > -24$ at 200°C) and uranium should have been dissolved in the form of U(VI) as uranyl complexes (Komninou & Sverjensky 1996). The reduction of U(VI) to U(IV) and subsequent UO_2 precipitation was spatially associated with graphite-rich basement-rooted faults and the basement-cover unconformity, which may have acted as redox interfaces (Hoeve & Quirt 1987).

X-ray absorption near-edge spectroscopy measurements show that the U in fluid inclusions remains in the form of U(VI) from 25°C to 150°C. This indicates that (i) the mechanical trapping of tiny UO_2 crystals within fluid inclusions could be ruled out as the origin of heterogeneity of U concentrations measured by LA-ICP-MS and SXRF and (ii) the heterogeneity of U concentration within fluid inclusions is related to the actual U(VI) content of the mineralising brines (Richard *et al.* 2010, 2012).

The present results differ from those of McCready *et al.* (2006) on a single fluid inclusion from McArthur River, which showed that the uranium is predominantly in the form of U(IV) in the inclusion. Further work on more fluid inclusions and different samples is required to resolve this disparity.

The noisy absorption signals do not permit interpretable EXAFS signals. One solution to this problem would be to find sufficiently U-rich fluid inclusions (100–1000 ppm U) for proper quantification. This constraint (coupled with the impossibility of analysing $CaCl_2$-rich brine inclusions) would be a limitation to the achievement of interpretable EXAFS signals because such U-rich inclusions are scarce, randomly distributed (Richard *et al.* 2010, 2012) and there are no means to estimate the U content of a given fluid inclusion by a nondestructive method prior to synchrotron experiments.

As a whole, the XANES data show that (i) at the time of fluid inclusion trapping, U was only present in the form of U(VI) (i.e. the most soluble form in these conditions); (ii) U remains in the U(VI) form during fluid inclusion cooling down to room temperature; and (iii) at sample scale, the coexistence of U(VI) species (within quartz-hosted fluid inclusions) and U(IV) species (as pitchblende mineralisation) highlights the drastic changes in redox conditions during the precipitation of quartz (more oxidising) and pitchblende (more reducing), the origin of the redox change remaining highly debated.

CONCLUSIONS AND PERSPECTIVES

Synchrotron X-ray fluorescence (SXRF) on fluid inclusions from the Rabbit Lake deposit allows reconstruction of the detailed K, Ca, Cr, Mn, Fe, Ni, Cu, Zn, Br, Sr, Cs, Ba, La, Ce, Pb and U composition of the mineralising NaCl-rich brine. This composition is comparable to that previously measured by laser ablation - inductively coupled plasma - mass spectrometry (LA-ICP-MS) on similar fluid inclusions from the McArthur River deposit and shows that the NaCl-rich brine is relatively homogeneous in composition among the studied deposits.

This study shows the great interest of combining SXRF analysis with non-negative matrix approximation (NNMA) during data processing, to obtain valuable information on element distribution within complex samples (quartz matrix + fluid inclusions + randomly distributed solids). This strategy was applied on one sample from the McArthur River deposit and allowed to clearly distinguish fluorescence signals from (i) the quartz matrix, which contains significant amounts of trace elements; (ii) Ce-La mineral inclusions; and (iii) fluid inclusions.

X-ray absorption near-edge spectroscopy (XANES) on four McArthur River sample fluid inclusions at room temperature and at 150°C (fluid inclusion trapping temperature) shows that (i) uranium has remained in the form of U(VI) (i.e. the most soluble form in these conditions) from trapping to present in the fluid inclusion and (ii) no UO_2 (U(IV)) precipitation was occurring within the brines at the time of fluid inclusion trapping.

Further work is needed to (i) understand the previously unreported decrepitation of $CaCl_2$-rich brine fluid inclusions under the X-ray beam; (ii) find sufficiently U-rich fluid inclusions (100–1000 ppm U) for proper quantification; and (iii) perform X-ray absorption experiments on U-rich fluid inclusions to get less noisy XANES signals, achieve more precise U-L3 edges to confirm the presence of U(VI) and possibly achieve interpretable extended X-ray absorption fine structure (EXAFS) signals. This is a prerequisite for a better understanding of U speciation and the nature of the ligands and the uranyl complexes in the brines responsible for the formation of the richest U deposits in the world.

ACKNOWLEDGEMENTS

We thank the European Synchrotron Radiation Facility (ESRF) ID22 beamline staff and especially R. Tucoulou for their precious technical help during experiments. P. Lach, M. Leisen and S. Fleurance are greatly thanked for their assistance. J. Dubessy and B. Aparicio are kindly acknowledged for preparation of the liquid standards. Samples were kindly provided by Areva NC and Cameco. Comments from two anonymous reviewers and editorial handling from C. Manning greatly improved the manuscript.

REFERENCES

Alexandre P, Kyser K, Polito P, Thomas D (2005) Alteration mineralogy and stable isotope geochemistry of Paleoproterozoic basement-hosted unconformity-type uranium deposits in the Athabasca Basin, Canada. *Economic Geology*, **100**, 1547–63.

Alexandre P, Kyser K, Thomas D, Polito P, Marlat J (2009) Geochronology of unconformity-related uranium deposits in the Athabasca Basin, Saskatchewan, Canada and their integration in the evolution of the basin. *Mineralium Deposita*, **44**, 41–59.

Annesley IR, Madore C, Portella P (2005) Geology and thermotectonic evolution of the western margin of the Trans-Hudson Orogen: Evidence from the eastern sub-Athabasca basement, Saskatchewan. *Canadian Journal of Earth Sciences*, **42**, 573–97.

Boiron MC, Cathelineau M, Richard A (2010) Fluid flows and metal deposition near basement/cover unconformity: lessons and analogies from Pb-Zn-F-Ba systems for the understanding of Proterozoic U deposits. *Geofluids*, **10**, 270–92.

Card CD, Pana D, Portella P, Thomas DJ, Annesley IR (2007) Basement rocks to the Athabasca Basin, Saskatchewan and Alberta. In: *EXTECH IV: Geology and Uranium EXploration TECHnology of the Proterozoic Athabasca Basin, Saskatchewan and Alberta* (eds Jefferson CW, Delaney G). *Geological Survey of Canada Bulletin*, **588**, 69–87.

Cauzid J, Philippot P, Somogyi A, Simionovici A, Bleuet P (2004) Quantification of single fluid inclusions by combining Synchrotron Radiation-Induced μ-X-ray Fluorescence and Transmission. *Analytical Chemistry*, **76**, 3988–94.

Cauzid J, Philippot P, Somogyi A, Ménez B, Simionovici A, Bleuet P (2006) Standardless quantification of single fluid inclusions using synchrotron radiation induced X-ray fluorescence. *Chemical Geology*, **227**, 165–83.

Cauzid J, Philippot P, Martinez-Criado G, Ménez B, Labouré S (2007) Contrasting Cu-complexing behaviour in vapour and liquid fluid inclusions from the Yankee Lode deposit, Mole Granite, Australia. *Chemical Geology*, **246**, 39–54.

Chiarenzelli J, Aspler L, Villeneuve M, Lewry J (1998) Early Proterozoic evolution of the Saskatchewan craton and its allochtonous cover, Trans-Hudson orogen. *Journal of Geology*, **106**, 247–67.

Cloutier J, Kyser K, Olivo GR, Alexandre P, Halaburda J (2009) The Millennium uranium deposit, Athabasca Basin, Saskatchewan, Canada: an atypical basement-hosted unconformity-related uranium deposit. *Economic Geology*, **104**, 815–40.

Cumming GL, Krstic D (1992) The age of unconformity-related uranium mineralization in the Athabasca Basin, Northern Saskatchewan. *Canadian Journal of Earth Sciences*, **29**, 1623–39.

Cuney M (2009) The extreme diversity of uranium deposits. *Mineralium Deposita*, **44**, 3–9.

Derome D, Cathelineau M, Cuney M, Fabre C, Lhomme T, Banks DA (2005) Mixing of sodic and calcic brines and uranium deposition at McArthur River, Saskatchewan, Canada: A Raman and laser-induced breakdown spectroscopic study of fluid inclusions. *Economic Geology*, **100**, 1529–45.

Fayek M, Kyser TK (1997) Characterization of multiple fluid-flow events and rare-earth-element mobility associated with formation of unconformity-type uranium deposits in the Athabasca Basin, Saskatchewan. *Canadian Mineralogist*, **35**, 627–58.

Fayek M, Kyser TK, Riciputi LR (2002) U and Pb isotope analysis of uranium minerals by ion microprobe and the geochronology of McArthur River and Sue Zone uranium deposits, Saskatchewan, Canada. *Canadian Mineralogist*, **40**, 1553–69.

Fontes JC, Matray JM (1993) Geochemistry and origin of formation brines from the Paris Basin, France 1. Brines associated with Triassic salts. *Chemical Geology*, **109**, 149–75.

Gaboreau S, Cuney M, Quirt D, Beaufort D, Patrier P, Mathieu R (2007) Significance of aluminum phosphate-sulfate minerals associated with U unconformity-type deposits: The Athabasca basin, Canada. *American Mineralogist*, **92**, 267–80.

Hazen RM, Ewing RC, Sverjensky DA (2009) Evolution of uranium and thorium minerals. *American Mineralogist*, **94**, 1293–311.

Hecht L, Cuney M (2000) Hydrothermal alternation of monazite in the Precambrian crystalline basement of the Athabasca Basin (Saskatchewan, Canada): Implications for the formation of unconformity-related uranium deposits. *Mineralium Deposita*, **35**, 791–5.

Heine TH (1986) The geology of the Rabbit Lake uranium deposit, Saskatchewan. In: *Uranium Deposits of Canada* (ed. Evans EL). *Canadian Institute of Mining, Metallurgy and Petroleum*, Special Volume, **33**, 134–43.

Hoeve J, Quirt DA (1987) A stationary redox front as a critical factor in the formation of high-grade, unconformity-type uranium ores in the Athabasca Basin, Saskatchewan, Canada. *Bulletin de Mineralogy*, **110**, 151–71.

Hoeve J, Sibbald TII (1978) On the genesis of the Rabbit Lake and other unconformity-type uranium deposits in Northern Saskatchewan, Canada. *Economic Geology*, **73**, 1450–73.

Jefferson CW, Thomas DJ, Gandhi SS, Ramaekers P, Delaney G, Brisbin D, Cutts C, Portella P, Olson RA (2007) Unconformity associated uranium deposits of the Athabasca Basin, Saskatchewan and Alberta. In: *EXTECH IV: Geology and Uranium EXploration TECHnology of the Proterozoic Athabasca Basin, Saskatchewan and Alberta* (eds Jefferson CW, Delaney G). *Geological Survey of Canada Bulletin*, **588**, 23–67.

Komninou A, Sverjensky DA (1996) Geochemical modeling of the formation of an unconformity-type uranium deposit. *Economic Geology*, **91**, 590–606.

Kotzer TG, Kyser TK (1995) Petrogenesis of the Proterozoic Athabasca Basin, northern Saskatchewan, Canada, and its relation to diagenesis, hydrothermal uranium mineralization and paleohydrogeology. *Chemical Geology*, **120**, 45–89.

Kyser TK, Cuney M (2008) *Recent and not-so-Recent Developments in Uranium Deposits and Implications for Exploration*. Mineralogical Association of Canada, Québec, 257 p.

Lee DD, Seung HS (1999) Learning the parts of objects by non-negative matrix factorization. *Nature*, **401**, 788–91.

Leisen M, Boiron MC, Richard A, Dubessy J (2012) Determination of Cl and Br concentrations in individual fluid inclusions by combining microthermometry and LA-ICPMS analysis: Implications for the origin of salinity in crustal fluids. *Chemical Geology*, **330–331**, 197–206.

Lowenstein TK, Timofeeff MN (2008) Secular variations in seawater chemistry as a control on the chemistry of basinal brines: test of the hypothesis. *Geofluids*, **8**, 77–92.

Martinez-Criado G, Tucoulou R, Cloetens P, Bleuet P, Bohic S, Cauzid J, Kieffer I, Kosior E, Labouré S, Petitgirard S, Rack A, Sans JA, Segura-Ruiz J, Suhonen H, Susini J, Villanova J (2012) Status of the hard X-ray microprobe beamline ID22 of the European Synchrotron Radiation Facility. *Journal of Synchrotron Radiation*, **19**, 10–8.

McCready AJ, Annesley IR, Cuney M, Cavell RG, Derome D, Rickers K, Webb MA (2005) Trace element geochemistry of fluid inclusions in the Athabasca Basin: implications and constraints on the metallogenesis of world-class uranium deposits. Jahresbericht/Hamburger Synchrotronstrahlungslabor HASYLAB am Deutschen Elektronen-Synchrotron DESY = Annual report, HASYLAB, 1117–8.

McCready AJ, Annesley IR, Cuney M, Cavell RG, Derome D, Rickers K, Letard I, Webb MA (2006) *Further Advancements in Understanding Uranium Metallogenesis and Fluid Flow in the Athabasca Basin: New Data From Synchrotron Analysis of Fluid Inclusions.* Geological Association of Canada – Mineralogical Association of Canada meeting, Montréal.

Ménez B, Philippot P, Bonnin-Mosbah M, Simionovici A, Gibert F (2002) Analysis of individual inclusions using synchrotron X-ray fluorescence microprobe: progress toward calibration for trace elements. *Geochimica et Cosmochimica Acta*, **66**, 561–76.

Mercadier J, Richard A, Boiron MC, Cathelineau M, Cuney M (2010) Migration of brines in the basement rocks of the Athabasca Basin through microfracture networks (P-Patch U deposit, Canada). *Lithos*, **115**, 121–36.

Mercadier J, Cuney M, Lach P, Boiron MC, Bonhoure J, Richard A, Leisen M, Kister P (2011) Origin of uranium deposits revealed by their rare earth element signature. *Terra Nova*, **23**, 264–9.

Mercadier J, Richard A, Cathelineau M (2012) Boron and magnesium-rich marine brines at the origin of giant unconformity-related uranium deposits: $\delta^{11}B$ evidence from Mg-tourmalines. *Geology*, **40**, 231–4.

Pagel M, Poty B, Sheppard SMF (1980) Contribution to some Saskatchewan uranium deposits mainly from fluid inclusion and isotopic data. In: *International Uranium Symposium on the Pine Creek Geosyncline* (ed. IAEA), pp. 639–54. IAEA, Vienna.

Philippot P, Ménez B, Chevallier P, Gibert F, Legrand F, Populus P (1998) Absorption correction procedures for quantitative analysis of fluid inclusions using synchrotron radiation X-ray fluorescence. *Chemical Geology*, **144**, 121–36.

Philippot P, Ménez B, Simionovici A, Chabiron A, Cuney M, Snigirev A, Snigireva I (2000) X-ray imaging of uranium in individual fluid inclusions. *Terra Nova*, **12**, 84–9.

Ramaekers P, Jefferson CW, Yeo GM, Collier B, Long DG, Catuneanu O, Bernier S, Kupsch B, Post R, Drever G, McHardy S, Jircka D, Cutts C, Wheatley K (2007) Revised geological map and stratigraphy of the Athabasca Group, Saskatchewan and Alberta. In: *EXTECH IV: Geology and Uranium EXploration TECHnology of the Proterozoic Athabasca Basin, Saskatchewan and Alberta* (eds. Jefferson CW, Delaney G). *Geological Survey of Canada Bulletin*, **588**, 155–91.

Richard A, Pettke T, Cathelineau M, Boiron MC, Mercadier J, Cuney M, Derome D (2010) Brine–rock interaction in the Athabasca basement (McArthur River U deposit, Canada): consequences for fluid chemistry and uranium uptake. *Terra Nova*, **22**, 303–8.

Richard A, Banks DA, Mercadier J, Boiron MC, Cuney M, Cathelineau M (2011) An evaporated seawater origin for the ore-forming brines in unconformity-related uranium deposits (Athabasca Basin, Canada): Cl/Br and $\delta^{37}Cl$ analysis of fluid inclusions. *Geochimica et Cosmochimica Acta*, **75**, 2792–810.

Richard A, Rozsypal C, Mercadier J, Banks DA, Cuney M, Boiron MC, Cathelineau M (2012) Giant uranium deposits formed from exceptionally uranium-rich acidic brines. *Nature Geoscience*, **5**, 142–6.

Ruzicka V (1989) Monometallic and polymetallic deposits associated with sub-Athabasca unconformity in Saskatchewan. *Geological Survey of Canada Paper*, **1–C**, 67–79.

Solé VA, Papillon E, Cotte M, Walter P, Susini J (2007) PyMCA: a multiplatform code for the analysis of energy-dispersive X-ray fluorescence spectra. *Spectrochimica Acta Part B*, **62**, 63–8.

GEOFLUIDS

Volume 13, Number 2, May 2013
ISSN 1468-8115

CONTENTS

WILEY
Blackwell

Geofluids* is abstracted/indexed in *Chemical Abstracts

This journal is available online at Wiley Online Library.
Visit onlinelibrary.wiley.com to search the articles and register for table of contents and e-mail alerts.